IET Renewable Power Generation

Research Article

IET Journals
The Institution of Engineering and Technology

Dynamic modelling and control for assessment of large-scale wind and solar integration in power systems

ISSN 1752-1416
Received on 14th April 2020
Revised 31st August 2020
Accepted on 21st September 2020
E-First on 4th February 2021
doi: 10.1049/iet-rpg.2020.0458
www.ietdl.org

Michael Kyesswa[1] ✉, Hüseyin Çakmak[1], Uwe Kühnapfel[1], Veit Hagenmeyer[1]

[1]Institute for Automation and Applied Informatics, Karlsruhe Institute of Technology, Karlsruhe, Germany

✉ *E-mail: michael.kyesswa@kit.edu*

Abstract: The integration of variable and unpredictable renewable energy sources into the current power networks introduces considerable changes in system operations. This poses enormous threats to the stability of the power system. Hence, it is essential to analyse the necessary adjustments in operation strategies in preparation for increased amounts of variable generation in existing power systems. The present study describes the dynamic modelling and integration of solar photovoltaic and wind power generation systems into a transient stability analysis toolbox. In view of the inherent connection of renewable energy generators to the electrical network through converter systems, the main contribution in the present study is the development of high-level control functions to model converter interfaces with reference to standard grid operation codes. The dynamic models and corresponding control functions are tested using a network representing the transmission grid of the Baden-Württemberg state in Germany as part of the assessment process to analyse the capability of the control functions for grid stability support. The simulation results show that the proposed converter control functions can equip renewable energy generators with equivalent features from a functional point of view to those of synchronous generators.

1 Introduction

Alternative energy from variable renewable energy sources, especially solar photovoltaic (PV) and wind energy, is widely considered to have great potential towards future low-carbon energy generation systems [1]. The actual trend also indicates a large growth in the global installed capacity of such sources over the past few years. For instance, the trend in the installed capacity in Germany from 2010 to 2018 shows a 149% increase in solar PV capacity from 17.94 to 44.59 GW and a 116% increase in wind power capacity from 27.18 to 58.73 GW, considering both onshore and offshore wind power [2]. A similar trend in the installed generation capacity is observed on the global scale as reported in [3, 4].

The integration of variable renewable energy sources, however, poses considerable challenges in the operation of the existing networks. From the power generation point of view, the primary energy sources are weather dependent and therefore, variable and highly unpredictable [5], which transforms into the continuous fluctuation of the generated power. In terms of grid interconnection, variable renewable energy generators are connected to the grid through converter interfaces rather than using synchronous machines applied in conventional generators. Synchronous machines are the main source of inertia, which contributes to system damping and thus determines the rate of change of system frequency following a disturbance. This capability is not inherently provided by the power electronic converters adapted for renewable energy sources [6]. Therefore, replacing conventional generators with more variable generators results in a decrease in system inertia and may leave the power system vulnerable to abrupt disturbances. Furthermore, the connection of variable renewable energy generators are mainly on the distribution level [7], which causes regulation challenges for system operators in maintaining the respective voltage profile within standard acceptable operating limits.

The challenges introduced in system operation, as highlighted above, introduce additional requirements in the power system analysis process. This has led to a greater need for dynamic modelling of renewable energy sources and the corresponding control systems in order to include such sources in the overall system stability analysis. As a result, numerous efforts have been undertaken in research and industry to address the need for representing renewable energy resources as inverter-based sources in system stability studies. References [8–11] present the general guidelines that have been defined to establish best practices for the generic modelling of renewable energy sources for dynamic simulations at various time scales. The survey in [12] on the prevailing international best practices on modelling inverter-based generation for power system dynamic studies shows that renewable energy sources can be represented by the following models: negative load (NL) models, root mean square (RMS) models, and electromagnetic transient (EMT)-based models. The choice of the model type is governed by the transient behaviour and time frame of interest during the analysis. It is reported that a number of system operators mainly use the NL type model, which neglects the dynamic behaviour of renewable energy sources during stability studies. RMS type models are applied for the electro-mechanical transient phenomenon for analysis of frequency, voltage and rotor angle stability. Due to the significance of the power electronic converters in the operation of inverter-connected generators, further research efforts have focused on including the power electronic converters in the dynamic model representation as presented in [13–15]. In the electro-mechanical phenomena, the time scale of interest shows that modelling the fast-switching transients of converters is not necessary. In this case, converters are represented by average models in RMS type models. In order to account for the switching transients of the power electronics and converter controls, detailed models of inverter-based generators are represented using EMT type models as described in [13, 14].

In addition to the general dynamic models of the renewable energy sources, recent grid specifications increasingly necessitate inverter-based generators to be equipped with network support capabilities such as voltage support, frequency support, and fault ride-through (FRT) in the event of network disturbances. Such requirements are defined by national and international standards for the interconnection of distributed generation sources, which include EN 50438, IEC 61727, IEC 62116, VDE V 0126-2, VDE-AR-N 4105, BDEW, and IEEE 1547 [13]. However, the generic models defined in the available specifications as part of the best practices for dynamic models of inverter-based generators do not include the functionality specified by grid codes as part of the interfacing converter models.

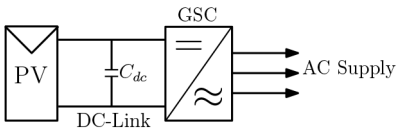

Fig. 1 *PV interface topology using single-stage conversion with GSC [7]*

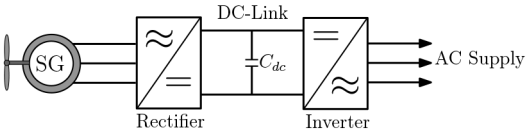

Fig. 2 *Schematic representation of wind power generation system consisting of a wind turbine, synchronous machine (SG), and fully rated converter system*

The main contribution of the present paper is the derivation of high-level converter functions based on standard grid operation codes as part of the converter control to achieve the necessary grid support functions, in addition to generic dynamic modelling of inverter-based generators. Furthermore, the derived models and control functions are implemented in a transient stability analysis tool based on an open-source toolbox Matdyn [16]. The goal of the implementation is to analyse the impact of the large-scale integration of renewable energy sources in the power system. In addition, the implemented functions are used to evaluate the required measures to maintain the network frequency within the normal operational limits in the presence of the continuous fluctuations in renewable energy generation.

The rest of the present paper is organised as follows: Section 2, describes the generic models of solar PV and Wind generation systems. The high-level control functions of the inverter are described in Section 3. An overview of the implementation aspects of the derived models in a transient stability analysis toolbox is given in Section 4. Section 5 presents the assessment results to analyse the functionality of the developed models and control functions. The conclusion of the paper is given in Section 6, including an outlook for future work.

2 Generic dynamic models

The current section describes the generic dynamic models of solar PV and wind power generation systems for transient stability simulations. The assumptions considered to simplify the models are also described.

2.1 Solar PV generation system

The PV generation system presented in this paper is based on a single-stage conversion system as shown in Fig. 1. In view of the differences in response times, PV components can be conveniently divided into steady-state and dynamic models. Steady-state models account for long-term effects and consider component variables, such as PV array power production and maximum power point tracking (MPPT), that are affected by variations in solar radiations and cell temperatures. Since the main focus in the present paper is on the short-term transient behaviour, the long-term steady-state PV components models are not considered. Dynamic models study short-term behaviour of power converters and converter controllers on a time scale of a few seconds. In deriving the dynamic models, the longer-term variables, such as solar radiation and the maximum power point, are assumed to be constant for the study period of the system dynamics following the time-scale separation principle based on the singular perturbation theory [17]. This simplifies the model of the PV array to a constant power source, for which the power value is determined at the initialisation stage from steady-state calculations.

2.1.1 PV system DC-link model: The DC-link is the interface between the PV-array and the inverter. In the present paper, the DC-Link is modelled under the assumption that the stationary maximum power point does not change during dynamics analysis. Thereby, the input power (P_{dc}) to the inverter is equal to the PV array output power (P_{pv}), which is equal to the maximum power point (P_{mpp}). The general condition for the steady-state initialisation of the PV model is given by

$$P_{\mathrm{ac}} = P_{\mathrm{inv}} = P_{\mathrm{dc}} = P_{\mathrm{mpp}} = P_{\mathrm{pv}} \tag{1}$$

where P_{ac} is the inverter active output power and P_{inv} is the inverter input power.

The PV array power P_{pv} is directly dependent on the array voltage. In the single-stage conversion system considered here, the array voltage is directly connected to the inverter. The dynamics of the DC link voltage are described from the relationship between the input power P_{dc} and the output power P_{inv} of the DC link given by

$$\frac{\mathrm{d}U_{\mathrm{dc}}}{\mathrm{d}t} = \frac{P_{\mathrm{dc}} - P_{\mathrm{inv}}}{C_{\mathrm{dc}} U_{\mathrm{dc}}} \tag{2}$$

In (2), U_{dc} is the DC-link voltage and C_{dc} is DC-link capacitance. The dynamic behaviour of the inverter DC side depends on the control of the inverter active current.

2.1.2 PV system grid-side converter (GSC): The PV DC-link voltage is converted to AC-grid voltage at a fixed frequency of the power grid using the GSC (inverter). The response of the PV generation system during network transients is defined by control functions of the inverter. The inverter model developed in this paper is based on standard grid operation codes which require inverter-connected generation sources to actively contribute to grid stability. The control functions developed for the GSC model are described in Section 3.

2.2 Wind power generation system

The commonly used configurations in wind power systems are fixed speed wind turbine with a squirrel cage induction generator, variable speed wind turbine with a doubly fed induction generator, and variable speed wind turbine with direct drive synchronous generator. Details of the components and operation of the generator systems are given in [18]. In the present paper, a variable speed wind turbine with a direct drive synchronous machine system is considered. Fig. 2 shows a generic representation of the generator system interfaced with the AC network.

In deriving the model, the mechanical power and rotational speed of the turbine are defined as inputs to the generator from the steady-state calculations. The input mechanical power is assumed to remain constant for the duration of the dynamic simulations following the time-scale separation principle. This is due to the fact that the wind speed, which defines the extracted power from the wind, does not change drastically in a few seconds. On the electrical side of the system, the synchronous generator is connected to the power grid through a full-scale frequency converter. As shown in Fig. 2, the converter system is made up of the generator-side converter (rectifier), a DC-link, and a GSC (inverter). The models of the individual short-term dynamic components of the wind power generation system are described in the following subsections.

2.2.1 Synchronous generator model: The synchronous generator considered in this paper is a permanent magnet synchronous generator (PMSG), which has the characteristic advantage of eliminating the need for a DC excitation system and slip rings, resulting in reduced losses and less maintenance requirements [19]. The dynamic model of the PMSG is described by (3)–(7).

$$\begin{aligned} u_{ds} &= -R_s i_{ds} - \omega_s \psi_{qs} + \frac{\mathrm{d}\psi_{ds}}{\mathrm{d}t} \\ u_{qs} &= -R_s i_{qs} + \omega_s \psi_{ds} + \frac{\mathrm{d}\psi_{qs}}{\mathrm{d}t} \end{aligned} \tag{3}$$

$$\begin{aligned}\psi_{ds} &= -L_{ds}i_{ds} + \psi_{\mathrm{pm}} \\ \psi_{qs} &= -L_{qs}i_{qs}\end{aligned} \tag{4}$$

The stator voltage equations are given by (3) defined in the rotor flux reference frame, where u_{ds} and u_{qs} are components of the stator terminal voltage, and i_{ds} and i_{qs} the components of the stator current in the d- and q-axis. R_s is the stator resistance and ω_s is the generator electrical angular speed. The d and q stator flux linkages ψ_{ds} and ψ_{qs} are given by (4) [20], where L_{ds} and L_{qs} are corresponding d and q stator leakage inductances, and ψ_{pm} is the permanent magnet flux leakage.

Equation (5) shows the calculation of the active power and reactive output power from the generators.

$$\begin{aligned}P_g &= \frac{3}{2}(u_{ds}i_{ds} + u_{qs}i_{qs}) \\ Q_g &= \frac{3}{2}(u_{qs}i_{ds} - u_{ds}i_{qs})\end{aligned} \tag{5}$$

$$\frac{\mathrm{d}\omega_m}{\mathrm{d}t} = \frac{1}{2H_m}(T_m - T_e) \tag{6}$$

$$T_e = \frac{3}{2}p\left[\psi_{\mathrm{pm}} + (L_q - L_d)i_{ds}\right]i_{qs} \tag{7}$$

The mechanical shaft of the generator is modelled using the equation of motion in (6). In the direct-drive system, the full-scale frequency converter is assumed to filter out the shaft dynamics. Thereby, all rotating masses are represented by an equivalent single shaft in the model. Equation (6) gives the resulting generator mechanical equation, where ω_m is the mechanical angular speed, H_m is the rotor inertia constant, and T_m is the mechanical torque. The electrical torque T_e in (6) is calculated according to (7).

2.2.2 Generator-side converter control: The generator-side converter is modelled as a fully controllable active pulse width modulated (PWM) insulated-gate bipolar transistor (IGBT) converter. However, the analysis in the present paper in based on the fundamental frequency assumptions; thereby, the high-switching frequency of the IGBTs are neglected following the time-scale separation principle. With this assumption, the generator-side converter is modelled using an average model.

The controller strategy applied in the converter is the full torque control strategy [19, 21], in which the total stator current is induced in the q-axis of the stator and the d-axis current is set to zero. Applying this to the expression in (7) results in maximum torque generation from the generator. Fig. 3 shows the separation of converter control in d- and q-axis current loops. The reference torque in the q-axis control loop is determined from MPPT. The generator-side converter controls the active power and voltage at the generator terminals.

From Fig. 3, the model of the q-axis control loop is given by (8). In reference to the full torque strategy, the d-axis control loop is modelled to regulate the value of the d-axis current to a reference current $i_{d,\mathrm{ref}} = 0$. This results in the controller equations given in (9).

$$\begin{aligned}i_{q,\mathrm{ref}} &= \frac{2T_{e,\mathrm{ref}}}{3p\psi_{\mathrm{pm}}}, \quad \frac{\mathrm{d}x_q}{\mathrm{d}t} = K_{i,q}(i_{q,\mathrm{ref}} - i_{qs}) \\ i_{qr} &= x_q + K_{p,q}(i_{q,\mathrm{ref}} - i_{qs}) - \omega_s C_r u_{ds}\end{aligned} \tag{8}$$

$$\begin{aligned}\frac{\mathrm{d}x_d}{\mathrm{d}t} &= K_{i,d}(i_{d,\mathrm{ref}} - i_{ds}) \\ i_{dr} &= x_d + K_{p,d}(i_{d,\mathrm{ref}} - i_{ds}) \\ &\quad + \omega_s C_r u_{qs}\end{aligned} \tag{9}$$

The parameters K_i and K_p are the integral and proportional gains of the proportional–integral controller corresponding control loops, while x_d and x_q are state variables within the control loops.

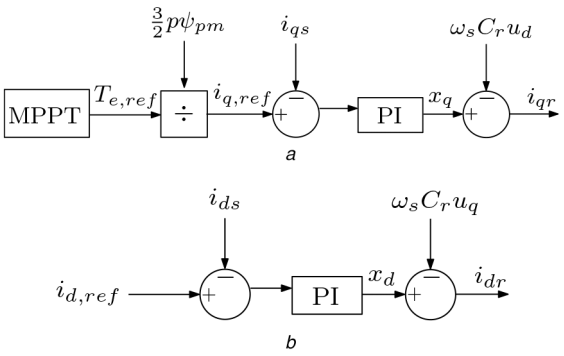

Fig. 3 *Generator-side converter control scheme*
(a) *q-axis current control with MPPT,* ***(b)*** *d-axis current control with zero direct-axis current control ($I_{d,\mathrm{ref}}$)*

The output signals i_{qr} and i_{dr} of the q- and d-axis control loops are used to control the PWM IGBTs of the rectifier.

In Fig. 3, the terms $\omega_s C_r u_{ds}$ and $\omega_s C_r u_{qs}$ are referred to as feed forward terms. These compensate for the cross coupling between the d- and q-control loops resulting from the transformation of the currents from the network reference frame to the rotating reference frame. Parameter C_r in (8) and (9) is the value of the shunt capacitor connected across the generator terminals.

2.2.3 Wind system DC-link model: The wind system storage element of the DC-link is similar to that in the PV system DC Link model described earlier. Assuming a lossless DC-link, the input DC power is equal to the generator-side active power P_g. Thereby, the DC-link model in this case is given by

$$\frac{\mathrm{d}U_{dc}}{\mathrm{d}t} = \frac{P_g - P_{\mathrm{inv}}}{C_{dc}U_{dc}} \tag{10}$$

In addition to the energy storage element, the wind system DC-link is modelled to include a braking chopper for protecting the DC-link from excess power. In case the wind energy system cannot inject all the active power into the grid, the DC-link discharges through the chopper circuit to keep the link voltage below a critical value and enable FRT capability. The change in power ΔP_{chp} of the chopper is approximated by a first-order transfer function given by

$$\Delta P_{\mathrm{chp}} = (P_g - P_{\mathrm{inv}})\left(1 - \mathrm{e}^{-\Delta t/\tau}\right) \tag{11}$$

where Δt is the time step, and τ is the chopper regulation time constant.

2.2.4 Wind system GSC: The GSC of the wind system is similar to that of the PV system since both are interfaced to the grid via an inverter. For this reason, the GSC functions described in Section 3 are applied for both systems. As mentioned before, the developed inverter functions for grid support are based on standard grid codes for control of the grid-side injected power and voltage.

3 Inverter high-level functions

The present section describes the developed control functions to model the dynamic response of the inverter. The inverter described in the following is a current source inverter. Low-level functions for controlling the switching devices are neglected in this model since the RMS type model is considered. The following high-level inverter control functions are developed for regulating the voltage at the generator terminal and the power into the grid as specified by standard grid codes: Active power reduction; Reactive power support; and FRT. The developed functions for each of the control modes are described in the following subsections.

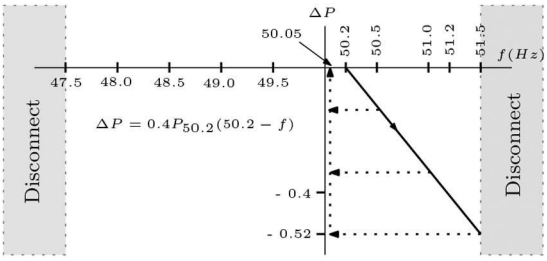

Fig. 4 *Frequency-dependent active power reduction profile [22]*

3.1 Active power reduction function

This control function is developed to represent the short-term frequency response of an inverter-connected system by reducing the active power injection if the frequency deviation is greater than a specified threshold, according to the grid code [22]. An example profile for active power injection is shown in Fig. 4, showing that the injected active power is reduced by 40% per frequency deviation greater than 0.2 Hz.

The active power reduction control function described in the present paper is based on a first-order transfer function simplification. The dynamic frequency f_{bus} at each bus is approximated by the expression in (12)

$$f_{\text{bus}} = f_0 + \frac{\mathrm{d}\theta_{\text{bus}}}{\mathrm{d}t} \tag{12}$$

$$f_{\text{inv},t} = f_{\text{inv},t-\Delta t} + (f_{\text{bus}} - f_{\text{inv},t-\Delta t})\left(1 - \mathrm{e}^{-\Delta t/\tau}\right) \tag{13}$$

where f_0 is the synchronous system frequency and $\mathrm{d}\theta_{\text{bus}}/\mathrm{d}t$ is the time derivative of the bus voltage angle. Using f_{bus} from (12), the frequency at the inverter terminal $f_{\text{inv},t}$ at time t is calculated as shown in (13), whereby $f_{\text{inv},t-\Delta t}$ is the inverter terminal frequency at the previous time step, Δt is the time step, and τ is time constant for frequency measurement.

The change in the injected inverter current $\Delta I_{d,q}$ (d- for active current and q- for reactive current) is calculated assuming a first order transfer function approximation as shown in (14)

$$\Delta I_{d,q} = (I_{dq,\text{ref}} - I_{dq,t-\Delta t})\left(1 - \mathrm{e}^{-\Delta t/\tau}\right) \tag{14}$$

$$I_{d,\text{ref}} = \frac{P_{\text{dc}}}{|U_{\text{inv}}|} \tag{15}$$

$$I_{d,\text{ref}} = \frac{P_{\text{act}} - \Delta P}{|U_{\text{inv}}|} \tag{16}$$

where $I_{dq,ref}$ is the nominal current of the respective controller, $I_{dq,t-\Delta t}$ is the current at a previous time step, and τ is the controller time constant. The value of the nominal active current $I_{d,\text{ref}}$ depends on the frequency deviation. If the frequency deviation is below the threshold value, the active current $I_{d,\text{ref}}$ is calculated from the specified power P_{dc} and the inverter bus voltage U_{inv} according to (15). For frequency deviations greater than the set threshold, $I_{d,\text{ref}}$ is calculated from the power P_{act} at the frequency threshold, the power deviation ΔP, and the voltage magnitude as shown in (16). The deviation ΔP is obtained from a power reduction profile according to standards set by network operators [23]. As shown in Fig. 4, operation standards require the generation system to be disconnected from the grid for frequency deviations < 47.5 Hz or >51.5 Hz [22], thus $I_{d,\text{ref}} = 0$.

3.2 Reactive power support function

The reactive power support control function is developed as a static grid support measure for voltage regulation. Grid operators specify the required reactive power according to either a set value (a constant reactive power in MVar or a constant power factor) or a characteristic curve (reactive power–voltage, reactive power–active power, and power factor–active power characteristics [22, 24]) depending on the plant operating point. In the presented inverter model, the reactive power value computed from the initial steady-state computations is directly applied for short-term dynamic simulations. For dynamic grid support measures, the nominal reactive current value is varied between constant current, given by the initial reactive current I_{q0} as shown in (17), and constant power depending on the initial reactive power Q_0 according to (18).

$$I_{q,\text{ref}} = I_{q0} \tag{17}$$

$$I_{q,\text{ref}} = -\frac{Q_0}{|U_{\text{inv}}|} \tag{18}$$

3.3 FRT function

The FRT control function is developed to support the grid during voltage sags caused by a fault condition according to a voltage support activation profile defined by the grid code as described in [23, 25]. In the developed FRT control function, the additional reactive current is injected into the grid to achieve voltage support. Equation (19) gives the expression for the calculation of the injected reactive current, where Δi_q is a normalised additional reactive current and Δu is the normalised voltage deviation.

$$\Delta i_q = k\Delta u \tag{19}$$

$$\Delta i_q = \frac{\Delta I_q}{|I_{\text{n}}|} \tag{20}$$

$$\Delta u_q = \frac{\Delta U}{|U_{\text{n}}|}; \Delta U = U - U_0 \tag{21}$$

The normalised value of the current is defined by the expression in (20), whereby ΔI_q is the required additional reactive current and I_{n} is the nominal reactive current. The normalised voltage deviation is given by (21), where ΔU is the absolute voltage deviation, U is the actual voltage value during the fault, U_0 is the voltage before the fault, and U_{n} is the nominal voltage. The parameter k is the reactive current–voltage gain, which represents the percentage increase of reactive current per percentage of the voltage drop [24]. As specified by the grid codes, the constant k can be set in the range 0–10 depending on the requirements defined by the network operator [26].

3.4 Inverter current limits

Different control functions contribute to the total active and reactive current outputs of the inverter as shown in the derived model. Equation (22) shows the contribution of each function, where $\Delta I_{d,\text{P}}$ is due to active power reduction, $\Delta I_{dq,\text{FRT}}$ due to FRT and $\Delta I_{q,\text{stat}}$ due to static reactive power control. The total inverter current is calculated from the active and reactive current components according to (23).

$$\begin{aligned} I_{d,\text{new}} &= I_{d,\text{old}} + \Delta I_{d,\text{P}} + \Delta I_{d,\text{FRT}} \\ I_{q,\text{new}} &= I_{q,\text{old}} + \Delta I_{q,\text{stat}} + \Delta I_{q,\text{FRT}} \end{aligned} \tag{22}$$

$$I_{\text{inv}} = \sqrt{I_{d,\text{new}}^2 + I_{q,\text{new}}^2} \tag{23}$$

The inverter power output is maintained within the inverter rating by using specified current limits. In the presented model, three cases are developed in order to maintain the injected current within the inverter rating conditions. In the first case (Case 1), the inverter reduces the injected active current as the reactive power requirement increases. The second case (Case 2) activates reduction of the injected reactive current to limit the total output. The third case (Case 3) reduces both active and reactive currents. However, in case of activated FRT operation, Case 1 is always

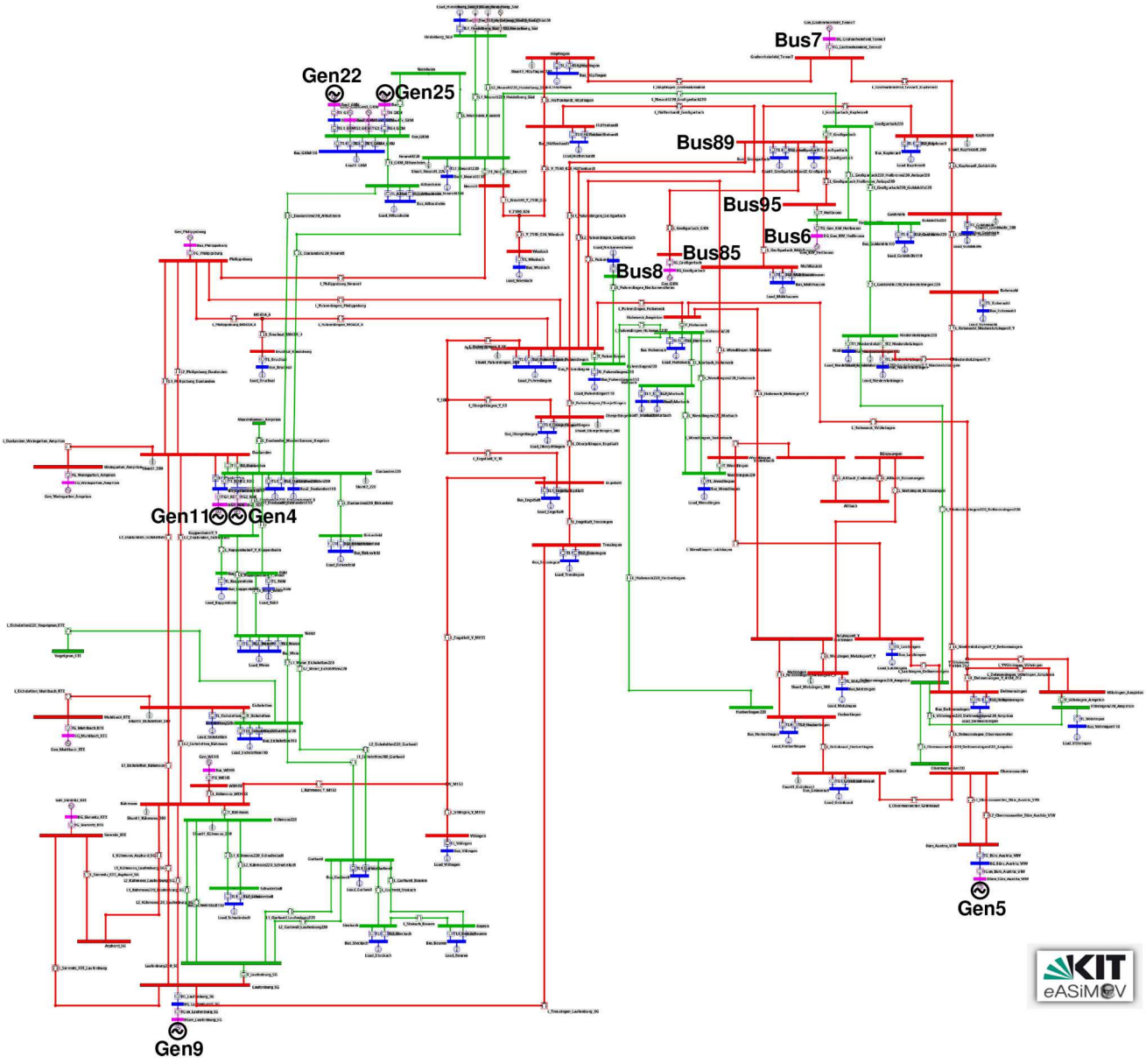

Fig. 5 *Structural representation of the Baden-Württemberg transmission network with modified generation to include renewable energy generators for testing purposes. Network model includes the Karlsruhe 110 kV and KIT Campus North 20 kV subnetworks*

applied to reduce the active current depending on the required reactive current.

4 Implementation in MatDyn

The models described in the previous sections are implemented in a Matlab-based transient stability analysis toolbox in order to analyse the dynamic response of the renewable energy sources. The extended toolbox is based on MatDyn [16], an open-source toolbox, which was developed to extend the use of MATPOWER [27] to transient stability analysis and time-domain simulation of power systems. MatDyn uses the MATPOWER power flow program for the steady-state calculations required at the initialisation stage of the dynamic simulations. The models are implemented in form of 'Matlab.m' files according to the MatDyn format. Implementation of the models in the extended simulation toolbox is similar to the MatDyn implemented components described in [16].

Parameters of each component are defined in the dynamic file, which are loaded at the beginning of the simulation along with the other dynamic parameters of the network. At the initialisation stage, power flow calculations are used to define the steady-state point of the system. For the new inverter-based components, an initialisation .m file is defined for each model to set the initial values of the corresponding dynamic states before the differential and algebraic equations are solved. The respective main blocks of the models are inverter and the DC-link file. In addition, the wind power system includes .m files for the PMSG generator and the generator-side converter. Details about the additional component models, solution methodology, and simulation workflow in the extended transient stability analysis toolbox are given in [28, 29].

5 Assessment of model integration

In the current section, simulation results are presented to illustrate the dynamic response and grid support capability of the proposed models. A network representing the transmission grid of the Baden-Württemberg state (see Fig. 5, network parameters from the online information published by the transmission grid operator https://www.transnetbw.com/en) is used for the presented simulation results. The original network consists of 17 generators, 149 buses, 225 branches and 49 loads. In the first test case, the performance of the control functions is analysed for grid support. The network is modified by replacing two synchronous generators with PV and wind power generators. A PV generator is connected to bus 5 and a wind power generator to bus 9. The second test case involves assessment of changes in system robustness, where four synchronous generators are replaced by renewable energy generators in the modified network. Since the purpose of the presented simulations is to analyse the interaction of renewable

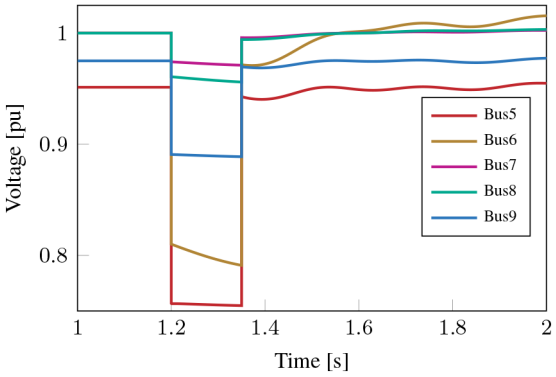

Fig. 6 *Bus voltage response during fault without grid support functionality*

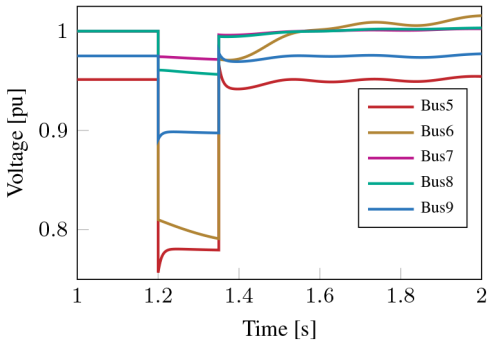

Fig. 7 *Bus voltage response during fault with grid voltage support functionality*

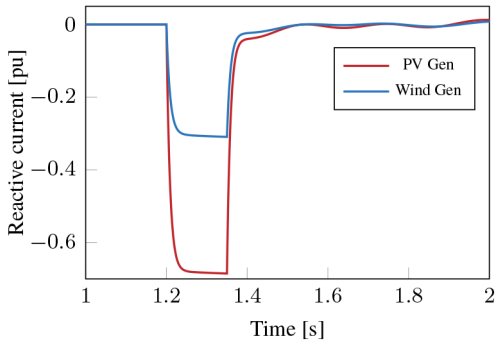

Fig. 8 *Injected reactive current for voltage support during fault*

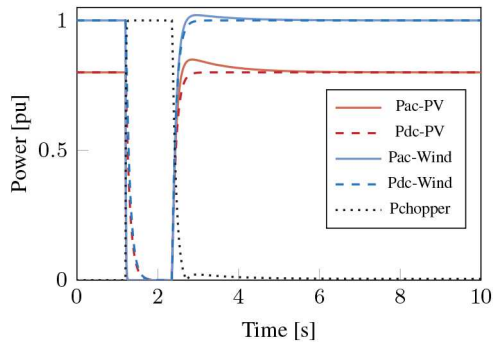

Fig. 9 *Response of AC and DC power for zero active power injection during fault*

energy generators with the network, the connected generators are assumed to be equivalent representations of the aggregated generators in a PV solar park and wind-farm.

5.1 Analysis of grid support functions

Initially, PV and wind power generators are connected without network support function during the fault period. In this mode, the renewable energy generators are set to disconnect from the network

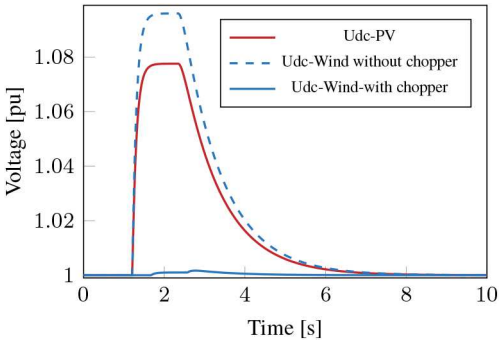

Fig. 10 *Response DC-side voltage during fault for zero-current mode*

during a fault condition. A three-phase short circuit fault is simulated on bus 95 at time $t = 1.2$ s and cleared after 150 ms. Fig. 6 shows the voltage response of selected generator buses following the fault. Important to observe is the voltage response on bus 5 and bus 9 connected to the PV and wind generators, respectively. The corresponding voltage magnitudes at buses 5 and 9 with respect to the nominal voltage are 79.6 and 91.4% at the beginning of the fault, and 79.3 and 91.2% after fault clearing, respectively.

In order to assess the grid support functions, the renewable energy generators are set to remain connected to the grid during the fault period. The inverters of the individual generator are set with FRT capability and voltage support with the $k = 4$ from (19). A similar fault is simulated as in the previous case. Fig. 7 shows the bus voltage response at selected network buses. As observed in the previous simulation case, there is a drop in voltage at all buses following the fault. The voltage magnitudes at the beginning of the fault are 79.6 and 91.4% of the nominal voltage, respectively, on bus 5 and bus 9. However, at the end of the fault, the respective voltage magnitudes lie at 82 and 92% of the nominal value. Therefore, there is an increase in bus voltage due to the injection of reactive power compared to the case without network support functionality. Fig. 8 shows the injected reactive current during the fault duration. The value of the current depends on the voltage drop and the gain constant k. Since the inverters are set with an equal gain constant ($k = 4$), the difference in the injected reactive current at bus 5 and bus 9 is due to the difference in the voltage drop at the buses according to the definition in (19). It is important to note that the effect of the voltage increase is also seen on other buses but depends on the distance from the respective inverter-connected bus.

Next, the response of the DC side of the inverter following the fault is investigated. For illustration purposes, the inverter control is such that the active power of the generators is set to zero during the fault. Fig. 9 shows the calculated power at the DC- and AC-side of the generators. The corresponding response in the DC-side voltage is shown in Fig. 10. Since the wind generator consists of a protection element in the DC-link, the level of the DC-side voltage is regulated within the limits of the link capacitor by dissipating the excess power through the braking chopper. This, in turn, regulates the generated power and angular rotational speed of the wind generator as shown in Figs. 11 and 12, respectively, in comparison to a case without the braking chopper in the DC-link. The power dissipated in the braking chopper is shown in Fig. 9. The responses in Figs. 11 and 12 show that the braking chopper enables the wind power generator to remain within the nominal operating conditions following a fault, which is important for FRT. At the end of the fault, the DC power is regulated to the MPP value, whereas the AC power is regulated so that the DC-side voltage returns to the nominal value as shown in Fig. 10.

In a further test, the active power reduction functionality is tested by simulating a load change of 10.5% of the total active power at $t = 1.2$ s. Fig. 13 shows the resulting frequency response in the system, where an increase in system frequency to a steady value of 50.44 Hz is observed resulting from a reduction in electrical power. The resulting reduction in the active power of the inverter-connected generators is shown in Fig. 14. As stated in the developed control function, the power reduction is triggered when the system frequency exceeds a threshold value (in this case, 50.2

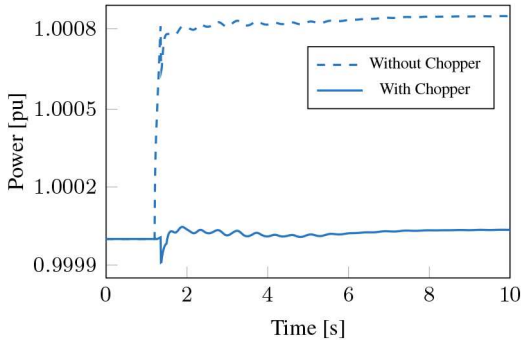

Fig. 11 *Wind generator output power*

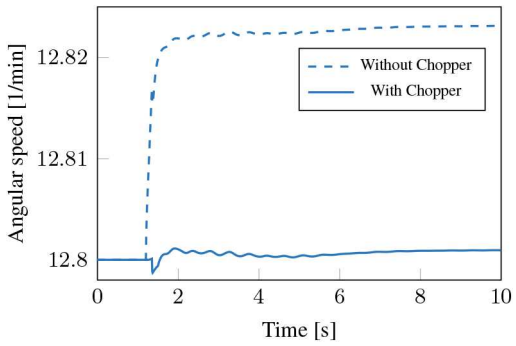

Fig. 12 *Wind generator mechanical angular speed*

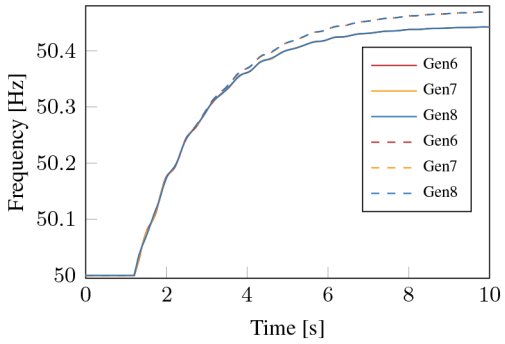

Fig. 13 *System frequency following a load change. Dashed lines show frequency without active power reduction and solid lines show frequency with active power reduction*

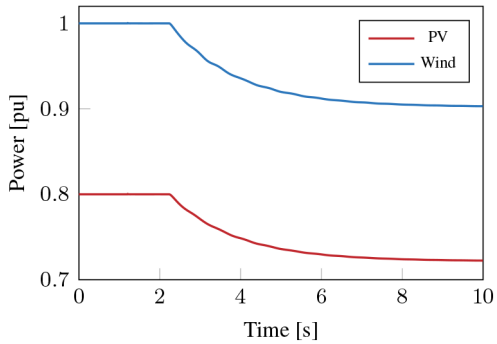

Fig. 14 *Active power reduction of the inverter-connected generators following a load change*

Hz). In this case, both generators reduce their active power injection by 10% of the value at 50.2 Hz. For comparison, the frequency response without power reduction is also plotted in Fig. 13 and shows a steady frequency value of 50.47 Hz. This shows that the active power reduction function of the inverter contributes to the regulation of system frequency.

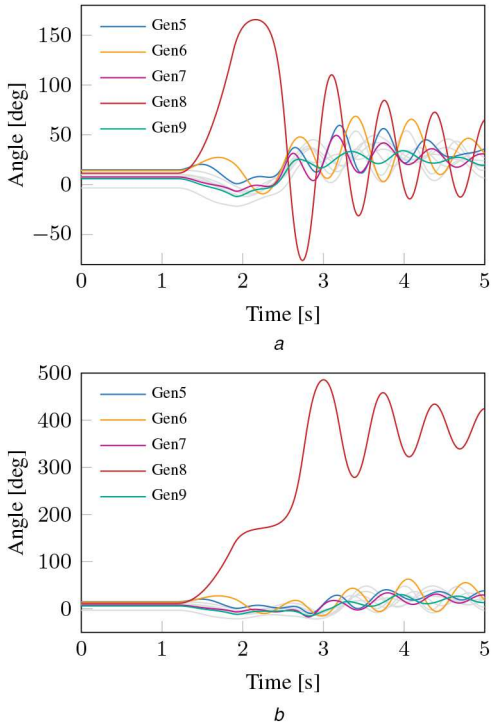

Fig. 15 *Generator rotor angle response*
(a) Stable system response for a fault cleared at the CCT of 681 ms, ***(b)*** Unstable system response for fault clearing beyond the CCT

5.2 Assessment of system robustness

In this section, the change in system robustness resulting from replacing synchronous machines with inverter-based renewable energy generation systems is analysed. Four synchronous machines in the original network are replaced with inverter-based generators as follows: PV generator on buses 4 and 22, and wind generator on buses 11 and 25. The number of inverter-based generators with grid support capability is varied and the system robustness is compared to the original network consisting of only synchronous machines. A three-phase fault is simulated on buses 85 and 89 in each case and the critical clearing time (CCT) is used as a measure of the system's robustness. The modified systems are summarised as follows:

- *System I*: Original network with 17 synchronous generators.
- *System II*: Modified network without FRT for all generators.
- *System III*: Modified with FRT for 1 generator (on bus 4) .
- *System IV*: Modified with FRT for 2 generators (4, 22) .
- *System V*: Modified with FRT for 3 generators (4, 11, 22) .
- *System VI*: Modified with FRT for all generators.

The CCT is obtained by varying the fault duration until the point where the system first attains unstable operation. Considering the original network in System I with the fault on bus 85, Fig. 15 depicts the rotor angle response of the selected generators at the CCT and beyond the CCT. The CCT is determined to be 681 ms. In reference to Fig. 5, the network instability, in this case, is due to the generator connected to bus 8 (represented by the red plot in Fig. 15) running out of synchronism with other generators. A similar analysis is carried out for the other test cases.

A summary of the CCTs for the different test systems is given in Table 1. The results in Table 1 show that the original network with only conventional synchronous generators has the highest CCT. This implies that the network is able to withstand a disturbance for a longer duration than the modified networks with integrated renewable energy generators. This behaviour can be attributed to the high system inertia provided by the synchronous machines, thereby reducing the rate of change of frequency following a disturbance. Fig. 16 further illustrates the above behaviour using the rate of angular separation of the critical

Table 1 Measure of system robustness using fault CCT

Test system	Critical clearing time, ms	
	Fault bus 85	Fault bus 89
System I	681	773
System II	622	698
System III	630	698
System IV	648	719
System V	655	720
System VI	676	744

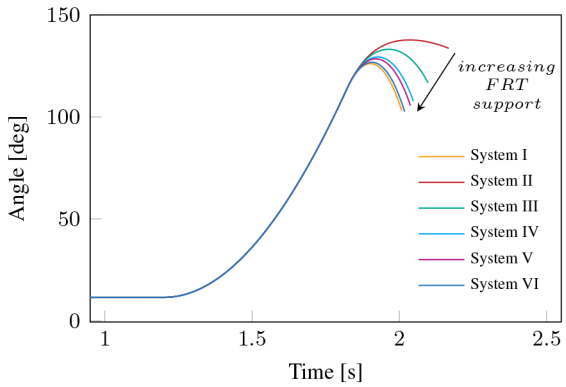

Fig. 16 *Change in rate of angular separation of the critical generator from the rest of the system with a varying number of inverter-connected generators providing FRT and voltage support*

generator from the rest of the generators following the fault in the different test systems. This represents the rate at which the corresponding system runs to instability. The critical generator is observed to experience a lower rate of angular separation in the original network (System I) compared to the modified networks.

The trend in the modified networks shows that the CCT increases with the number of inverter-based generators connected to the system with grid support functions as shown in Table 1. In addition, the rate at which the system runs to instability (i.e. the rate of angular separation of the critical generator) also decreases with an increasing number of generators providing FRT and grid support during the fault as shown in Fig. 16. Table 1 further shows that a similar trend is observed for the additional fault case on bus 89 but with different CCTs, as expected, due to a change in fault location. This ,therefore, implies that there is the potential improvement in system robustness if renewable energy generators are controlled to provide network support during disturbances.

5.3 Discussion

Considering the electrical response and neglecting the effects of the energy source at the grid interconnection point, the dynamic behaviour of inverter-interfaced generators is determined by the settings of the converter system. For the electromechanical phenomena considered in the present paper, the response of the inverter-connected generators during the transient period is determined by the high-level functions of the inverters as specified by the grid codes. The presented results show that the developed functions correctly represent the required functionality to support the network through active power injection for regulating the network frequency, reactive power injection for regulating the voltage, and FRT for network support during system disturbances.

Furthermore, the level of system robustness in the modified network with integrated renewable energy sources is shown to improve as the number of renewable energy generators connected with network support functionality increases. Therefore, correct settings of the interfacing converter functions in compliance with standard grid codes and network operator requirements provide the renewable energy generators with characteristics that can replicate the behaviour of synchronous generators from a functionality point of view as seen from the grid interconnection point.

6 Conclusion

The present paper describes the dynamic modelling and integration of solar PV and wind power generation systems in the time-domain simulation of power systems. The developed models are based on the notion that the dynamics of the converter perform the main role in the interaction of the renewable generators with the rest of the power system. The main contribution in the present paper is the development of the converter high-level functions based on grid standards for network support capability in the generic models used for transient stability analysis. The models are implemented and tested in a transient stability analysis toolbox. Simulation results show that renewable energy sources complying with network operator requirements contribute to grid stability support. The control functions of the interfacing converters provide renewable energy generation systems with features comparable to synchronous generators from a functional point of view. Future work will consider the comparison of the model performance to existing models in commercial software packages and validation of the control functions based on measured data from real plants. In addition, the full wind power system will be considered in future models in order to analyse the response and influence of tower dynamics on the overall system.

7 Acknowledgments

This work is part of the ‘Energy System 2050’ initiative of the Helmholtz Association.

8 References

[1] Graabak, I., Korpås, M.: ‘Variability characteristics of European wind and solar power resources – a review’, *Energies*, 2016, **9**, p. 449
[2] Fraunhofer ISE: ‘Energy charts,’ 08 Sep. 2018. Available at https://www.energy-charts.de/power_inst.htm, accessed 25 September 2018]
[3] REN21: ‘Renewables 2018 global status report,’ REN21 Secretariat, Paris, 2018
[4] IRENA: ‘Renewable capacity statistics 2019’ International Renewable Energy Agency (IRENA), 2019
[5] Huber, M., Dimkova, D., Hamacher, T.: ‘Integration of wind and solar power in Europe: assessment of flexibility requirements’, *Energy*, 2014, **69**, pp. 236–246
[6] D'Arco, S., Suul, J.A., Fosso, O.B.: ‘A virtual synchronous machine implementation for distributed control of power converters in SmartGrids’, *Electr. Power Syst. Res.*, 2015, **122**, pp. 180–197
[7] Xiao, W.: ‘*Photovoltaic power system: modeling, design, and control*’ (Wiley, Sydney, 2017)
[8] Western Electricity Coordinating Council (WECC) Renewable Energy Modeling Task Force: ‘Generic solar photovoltaic system dynamic simulation model specification,’ September 2012
[9] Western Electricity Coordinating Council (WECC) Renewable Energy Modeling Task Force: ‘WECC PV power plant dynamic modeling guidelines,’ April 2014
[10] Elliott, R., Ellis, A., Pourbeik, P.*, et al.*: ‘Generic photovoltaic system models for WECC – a status report’. 2015 IEEE Power & Energy Society General Meeting, Denver, CO, USA, July 2015, pp. 1–5
[11] Joint Working Group C4/C6.35/CIRED: ‘Modelling of inverter-based generation for power system dynamic studies,’ May 2018
[12] Lammert, G., Yamashita, K., Ospina, L.D.P.*, et al.*: ‘International industry practice on modelling and dynamic performance of inverter based generation in power system studies’, *CIGRE Sci. Eng.*, 2017, **8**, pp. 25–37
[13] Parvez, M., Elias, M., Rahim, N.*, et al.*: ‘Current control techniques for three-phase grid interconnection of renewable power generation systems: a review’, *Sol. Energy*, 2016, **135**, pp. 29–42
[14] Sau-Bassols, J., Prieto-Araujo, E., Galceran-Arellano, S.*, et al.*: ‘Operation and control of a current source converter series tapping of an LCC-HVDC link for integration of offshore wind power plants’, *Electr. Power Syst. Res.*, 2016, **141**, pp. 510–521
[15] Aziz, A., Amanullah, M.T.O., Stojcevski, A.: ‘Full converter based wind turbine generator system generic modelling: variations and applicability’, *Sustain. Energy Technol. Assess.*, 2016, **14**, pp. 46–62
[16] Cole, S., Belmans, R.: ‘MatDyn, a new Matlab-based toolbox for power system dynamic simulation’, *IEEE Trans. Power Syst.*, 2011, **26**, (3), pp. 1129–1136
[17] Kokotovic, P., Khali, H.K., O'reilly, J.: ‘*Singular perturbation methods in control: analysis and design*’, (SIAM, Philadelphia, 1999), **25**
[18] Machowski, J., Bialek, J.W., Bumby, J.R.: ‘*Power system dynamics, stability and control*’ (John Wiley & Sons, Ltd, Chichester, 2008)
[19] Michalke, G., Daniela, H.A., Hartkopf, T.: ‘Control strategy of a variable speed wind turbine with multipole permanent magnet synchronous generator’. European Wind Energy Association (EWEA), Brussels, 2007
[20] Eremia, M., Shahidehpour, M.: ‘*Handbook of electrical power system dynamics: modeling, stability, and control*’ (IEEE; Wiley, Hoboken, NJ, 2013)

[21] Chinchilla, M., Arnaltes, S., Burgos, J.: 'Control of permanent-magnet generators applied to variable-speed wind-energy systems connected to the grid', *IEEE Trans. Energy Convers.*, 2006, **21**, (1), pp. 130–135
[22] BDEW: '*Guideline for generating plants' connection to and parallel operation with the medium-voltage network*', BDEW Bundesverband der Energie- und Wasserwirtschaft e.V, Berlin, June 2008
[23] Commission Regulation (EU) 2016/631: 'Establishing a network code on requirements for grid connection of generators', *Off. J. Eur. Union*, 2016, **631**, pp. 1–68
[24] IEEE Std 1547-2018 (Revision of IEEE Std 1547-2003): 'IEEE Standard for interconnection and interoperability of distributed energy resources with associated electric power systems interfaces', 2018, pp. 1–138
[25] TransmissionCode 2007: 'Network and system rules of the German transmission system operators'. Verband der Netzbetreiber – VDN – e.V. beim VDEW, Berlin, August 2007
[26] Sourkounis, C., Tourou, P.: 'Grid code requirements for wind power integration in Europe'. Power Options for the Eastern Mediterranean Region, Limassol, Cyprus, November 2012
[27] Zimmerman, R.D., Murillo-Sanchez, C.E., Thomas, R.J.: 'MATPOWER: steady-state operations, planning, and analysis tools for power systems research and education', *IEEE Trans. Power Syst.*, 2011, **26**, (1), pp. 12–19
[28] Kyesswa, M., Çakmak, H., Kühnapfel, U.*, et al.*: 'A Matlab-based dynamic simulation module for power system transients analysis in the eASiMOV framework'. European Modelling Symp., Manchester, UK, November 2017
[29] Kyesswa, M., Çakmak, H., Kühnapfel, U.G.*, et al.*: 'A matlab-based simulation tool for the analysis of unsymmetrical power system transients in large networks'. European Conf. on Modelling and Simulation, Wilhelmshaven, Germany, May 2018
[30] Cole, S.: 'MatDyn documentation,Version 1.2,' February 2010